A High-Order Localized Artificial Diffusivity Scheme for Discontinuity Capturing on 1D Drift-Flux Models for Gas-Liquid Flows

Adyllyson H. Nascimento and Eugênio S. Rosa*

Department of Energy, School of Mechanical Engineering, University of Campinas, Campinas, Brazil

Abstract. A computational code is developed for the numerical solution of one-dimensional transient gas-liquid flows using drift-flux models, in isothermal and also with phase change situations. For these two-phase models, classical upwind schemes such as Roe- and Godunov-type schemes are generally difficult to derive and expensive to use, since there are no treatable analytic expressions for the Jacobian matrix, eigenvalues and eigenvectors of the system of equations. On the other hand, the high-order compact finite difference scheme becomes an attractive alternative on these occasions, as it does not make use of any wave propagation information from the system of equations. The present paper extends the localized artificial diffusivity method for high-order compact finite difference schemes to solve two-phase flows with discontinuities. The numerical method has simple formulation, straightforward implementation, low computational cost and, most importantly, high-accuracy. The numerical methodology proposed is validated by solving several numerical examples given in the literature. The simulations are sixth-order accurate and it is shown that the proposed numerical method provides accurate approximations of shock waves and contact discontinuities. This is an essential property for simulations of realistic mass transport problems relevant to operations in the petroleum industry.

1 Introduction

The investigation of gas-liquid flows has become increasingly important in engineering design and applications in petroleum, chemical, geothermal and nuclear industries.

---

*Corresponding author.
Emails: adyllyson@gmail.com (A. Nascimento), erosa@fem.unicamp.br (E. Rosa)

Mathematical modeling under steady-state and transient conditions is of great importance for flow prediction in terms of pressure, temperature, phase velocities and phase holdups. It is possible to predict steady-state flow along hilly terrains, as well as in transient flows for shut-off or re-start the line. The design of a new line or the shut-off or re-start lines requires the numerical solution of the mass, momentum and energy conservation equations.

Due to the complexity of gas-liquid flows, different two-phase models have been proposed in the literature to model the phenomena inherent to such flows [1, 39, 46]. A category of models that has been widely used to simulate gas-liquid flows is the drift-flux two-phase models. Several works in the literature use the drift-flux two-phase models with the hypothesis of isothermal flow, so the model has three equations, being a mass equation for each phase and a momentum equation for the gas-liquid mixture [32,38,56]. The latter results from the sum of the momentum equations for each phase, implying the elimination of complex modeling interfacial terms. However, this introduces the need for a closure law regarding the slip between the phases [57]. An advantage of the drift-flux model is that the system of equation is intrinsically stable.

The complexity of the closure laws severely restricts the possibilities of constructing numerical schemes that explicitly incorporate the physics of wave propagation into their formulations [17, 19, 44]. This is due to the difficulties in obtaining an analytical expression of the Jacobian matrix through purely algebraic manipulations. Nevertheless, some numerical schemes have been proposed for the isothermal drift-flux model. Romate [44] presented an approximate Riemann solver of Roe using a fully numerical approach. Evje and Fjelde [18] proposed an AUSM scheme that is not based on algebraic manipulation of the Jacobian, but makes explicit use of the approximate eigenvalues associated with the non-linear waves. Flåtten and Munkejord [22] derived a Roe-type Riemann solver with a linearized form of the Jacobian matrix obtained analytically. However, the eigenvalues were evaluated numerically. Santim and Rosa [45] also proposed a Roe-type Riemann solver, presenting an approximate analytical form for both the Jacobian matrix and the eigenvalues of the system. It is worth mentioning that all the numerical schemes mentioned above are at best second-order accurate.

To model the interfacial mass transfer between the phases it is necessary to add the energy conservation equation to the two-phase models. These models differ mainly in the level of disequilibrium between the two phases that they are able to take into account. The most complete model has seven equations [3], with an equation for the balances of mass, momentum and energy for each phase, in addition to an advection equation for the volume fraction. This model allows for the disequilibrium of pressure, temperature, velocity and Gibbs free energy between phases. Adding some equilibrium hypothesis reduces the number of equations needed in the two-phase models. The simplest model is the homogeneous equilibrium model (HEM) [9], which assumes that the phases have the same velocity and are in fully thermodynamic equilibrium. This model has three equations referring to the gas-liquid mixture, being the mass, momentum and energy conservation equations. One level of hierarchy above the HEM model is the homoge-

neous relaxation model (HRM) [9, 16], which considers a gas-liquid mixture that it is in thermodynamic equilibrium, but considers the chemical disequilibrium between the phases. The system of equations is augmented by a fourth equation referring to the mass conservation for one of the phases, where a source term models the mass transfer between the phases. Most of the two-phase models presented in the literature that consider phase change use a single velocity for the phases in their formulations [10, 36, 47, 48].

In this paper, gas-liquid flows are treated using two drift-flux models: isothermal and non-isothermal (with phase change). Since in this model the phase velocities differ, there is no exact or approximate expression for the eigenvalues and eigenvectors of the system of equations [50]. Consequently, the use of classical high-order schemes to capture discontinuities, such as WENO [28], also becomes computationally complicated, since WENO reconstruction is often performed in the characteristic space to avoid spurious oscillations [41]. On the other hand, an attractive alternative to capture discontinuities, using high-order compact finite difference schemes, has been proposed by Cook and Cabot [13, 14]. The method is based on the idea of dynamically adding localized artificial diffusivity when necessary, whereas a high-order compact finite difference scheme resolves the broad range of scales in flows. The capability of this approach to accurately treats shock-turbulence interaction was successfully demonstrated by several authors [20, 30].

The objective of this paper is to extend high-order compact finite difference schemes with the localized artificial diffusivity method to solve gas-liquid flows with two-phase drift-flux models. To the best of our knowledge, there are no studies related to the drift-flux two-phase models with the numerical methodology proposed. These numerical methods are particularly interesting because of their simple formulation, straightforward implementation, low computational cost and, most importantly, high-accuracy. The numerical methodology proposed is validated by solving several numerical examples given in the literature.

2 Two-phase flow models

The mathematical models that describe two-phase flows are conventionally obtained through some averaging procedure, in order to avoid excessive computational complexity. However, there is a significant loss of information associated with the averaging process. Consequently, additional information must be provided to the system of equations in the form of closure laws. Different formulations of two-phase flow models can be obtained based on different physical assumptions of the closure laws [1, 39, 46].

A general transient two-phase flow problem can be formulated using a two-fluid model or a drift-flux model, depending on the degree of dynamic coupling between the phases. In the two-fluid model, each phase is considered separately and the model is formulated in terms of two sets of conservation laws that govern the mass, momentum and energy balances of each phase. However, the introduction of two momentum equa-

tions in the formulation of the two-fluid model presents difficulties due to mathematical complications, and hyperbolicity may be lost due to the improper specification of interfacial interaction terms between the two-phases. The loss of hyperbolicity usually leads to an ill-posed problem which, in turn, can produce instabilities in numerical calculations. Consequently, careful studies of the interfacial constitutive equations are generally needed in the formulation of the two-fluid model [15, 46].

These difficulties associated with the two-fluid model can be significantly reduced by formulating two-phase problems in terms of the drift-flux model. In this model, the motion of the entire mixture is expressed by the momentum equation of the mixture and relative motion between the phases is taken into account by a kinematic constitutive equation. Although the complexity of the drift-flux model is an impediment to deriving exact hyperbolicity conditions, the drift-flux model has been shown to be hyperbolic for a reasonable range of parameters and fluid properties. Approximate hyperbolicity conditions of the drift-flux model valid for the Zuber-Findlay law have been presented in the literature [22, 44]. The use of the drift-flux model is appropriate when the motions of two phases are strongly coupled.

2.1 Isothermal drift-flux model

The drift-flux model is derived from the two-fluid model, where, in the momentum equation, the interfacial pressure is assumed to be the same for both phases. Next, the gas and liquid momentum equations are added to produce a mixture momentum equation. Thus, the drift-flux model for one-dimensional isothermal transient gas-liquid flow without phase change consists of two mass equations (gas and liquid phases) and a momentum equation (gas-liquid mixture) [22]:

$$\frac{\partial}{\partial t}\left(\alpha\rho_g\right)+\frac{\partial}{\partial x}\left(\alpha\rho_g u_g\right)=0, \tag{2.1a}$$

$$\frac{\partial}{\partial t}\left[(1-\alpha)\rho_l\right]+\frac{\partial}{\partial x}\left[(1-\alpha)\rho_l u_l\right]=0, \tag{2.1b}$$

$$\frac{\partial}{\partial t}\left[\alpha\rho_g u_g+(1-\alpha)\rho_l u_l\right]+\frac{\partial}{\partial x}\left[\alpha\rho_g u_g^2+(1-\alpha)\rho_l u_l^2+p\right]=s_m, \tag{2.1c}$$

where the subscripts g and l refer to the gas and liquid phases, ρ is the density, α is the void fraction, u is the velocity, and p is the common pressure for both phases. The source term of the momentum equation s_m includes terms of the frictional force of the mixture on the wall and the gravitational force:

$$s_m=-f_{TF}\frac{\rho_m|u_m|u_m}{2D}-\rho_m g\sin(\theta), \tag{2.2}$$

where $\rho_m=\alpha\rho_g+(1-\alpha)\rho_l$ is the mixture density, $u_m=\alpha u_g+(1-\alpha)u_l$ is the mixture velocity, D is the internal diameter, g is the gravitational constant and θ is the pipe inclination measured from the horizontal position.

The two-phase friction factor f_{TF} depends on the flow regime and is based on the mixture Reynolds number Re_m define as:

$$\text{Re}_m = \frac{\rho_m |u_m| D}{\mu_m}, \tag{2.3}$$

where $\mu_m = \alpha\mu_g + (1-\alpha)(1+2.5\alpha)\mu_l$ is the effective mixture viscosity [5].

For laminar flows ($\text{Re}_m \leq 2100$) the two-phase friction factor will be given by

$$f_{TF} = \frac{64}{\text{Re}_m}. \tag{2.4}$$

On the other hand, in turbulent flows with $\text{Re}_m > 2100$, the implicit correlation proposed by Colebrook is used to calculate the two-phase friction factor:

$$\frac{1}{\sqrt{f_{TF}}} = -2\log\left(\frac{\epsilon/D}{3.7} + \frac{2.51}{\text{Re}_m\sqrt{f_{TF}}}\right), \tag{2.5}$$

where ϵ represents the equivalent roughness of the pipe. To calculate the two-phase friction factor with this implicit correlation, an initial estimate was obtained with the Haaland correlation:

$$\frac{1}{\sqrt{f_{TF}}} = -1.8\log\left[\left(\frac{\epsilon/D}{3.7}\right)^{1.11} + \frac{6.9}{\text{Re}_m}\right]. \tag{2.6}$$

2.1.1 Closure laws

Both gas and liquid can be considered to be compressible. Thus, the thermodynamic state equations for the densities of the gas and liquid phases comes from the hypothesis of isothermal flow with pressure equilibrium between the phases, in the form:

$$\rho_l = \rho_{l,0} + \frac{p - p_{l,0}}{c_l^2} \quad \text{and} \quad \rho_g = \frac{p}{c_g^2}, \tag{2.7}$$

where c_l and c_g are the speed of sound in the liquid and the gas, respectively, and $\rho_{l,0}$ and $p_{l,0}$ are given as constants.

The other closure law is the kinematic relation between the phases proposed by Zuber and Findlay [57], which establishes a general expression in the form:

$$u_g = C_0[\alpha u_g + (1-\alpha)u_l] + v_d, \tag{2.8}$$

where C_0 and v_d are the so-called distribution parameter and drift velocity, respectively, which depend on the flow pattern. The validity of the relation (2.8) is limited to bubble and slug flow patterns. However, for these flow regimes, the Zuber and Findlay relation has been experimentally verified for a broad range of parameters proposed in the literature [6, 8, 11, 23, 27].

2.2   Adiabatic drift-flux model with phase change

As described in Section 2.1, the drift-flux model can be obtained from the two-fluid model, where in particular, the pressures in both phases are assumed to be equal, i.e., $p_g = p_l = p$. Thus, the momentum equations for each phase can be combined into a single momentum equation for the two-phase mixture. Additionally, with the assumption that the phase temperatures are equal, $T_g = T_l = T$, the energy equations for each phase can also be combined into an equation for the two-phase mixture. The resulting one-dimensional drift-flux model is then given by

$$\frac{\partial}{\partial t}\left(\alpha\rho_g\right)+\frac{\partial}{\partial x}\left(\alpha\rho_g u_g\right)=\Gamma, \tag{2.9a}$$

$$\frac{\partial}{\partial t}\left[(1-\alpha)\rho_l\right]+\frac{\partial}{\partial x}\left[(1-\alpha)\rho_l u_l\right]=-\Gamma, \tag{2.9b}$$

$$\frac{\partial}{\partial t}\left[\alpha\rho_g u_g+(1-\alpha)\rho_l u_l\right]+\frac{\partial}{\partial x}\left[\alpha\rho_g u_g^2+(1-\alpha)\rho_l u_l^2+p\right]=s_m, \tag{2.9c}$$

$$\frac{\partial}{\partial t}\left[\alpha E_g+(1-\alpha)E_l\right]+\frac{\partial}{\partial x}\left[\alpha E_g u_g+(1-\alpha)E_l u_l+u_m p\right]=s_e, \tag{2.9d}$$

where $E_k = \rho_k\left(e_k+u_k^2/2\right)$ is the total energy of each phase, which includes the specific internal energy e_k and the kinetic energy term $u_k^2/2$. The term Γ corresponds to the mass transfer between the phases. The source term of the momentum equation s_m is the same as already defined in Eq. (2.2), while the source term of the energy equation s_e only incorporates gravitational effects due to the weight of the two-phase mixture, and is defined as follows:

$$s_e = -\rho_m u_m g\sin(\theta). \tag{2.10}$$

The system of Eqs. (2.9a)-(2.9d) considers that the phases are in mechanical and thermal equilibrium, but takes into account the chemical disequilibrium between the phases. The phase change term Γ is usually expressed as [21]:

$$\Gamma = \mathcal{K}(\mu_l-\mu_g), \tag{2.11}$$

where μ_k are the chemical potentials of each phase and $\mathcal{K}$ is associated with a characteristic relaxation time for mass transfer between phases. Since $\mathcal{K} > 0$, the relaxation term leads the phases asymptotically towards equilibrium in Gibbs free energy. The relaxation term for a two-phase mixture depends on the interfacial area between the phases, making its determination quite difficult [48].

To circumvent this difficulty, it can be considered that the mass transfer is instantaneous, i.e, the limit $\mathcal{K} \to \infty$ (zero relaxation time) is taken, so that the relaxation for thermodynamic equilibrium is immediate. This limit is equivalent to explicitly assuming that $\mu_l = \mu_g$, so that this relation holds only in the two-phase region and the gas-liquid mixture is in the saturation region. Since $\mathcal{K} \to \infty$ and $\mu_l = \mu_g$, the product $\mathcal{K}(\mu_l-\mu_g)$ is

an indefinite limit. However, this can be solved by adding the mass equations (2.9a) and (2.9b), resulting in the following system of equations:

$$\frac{\partial}{\partial t}\left[\alpha\rho_g+(1-\alpha)\rho_l\right]+\frac{\partial}{\partial x}\left[\alpha\rho_g u_g+(1-\alpha)\rho_l u_l\right]=0, \tag{2.12a}$$

$$\frac{\partial}{\partial t}\left[\alpha\rho_g u_g+(1-\alpha)\rho_l u_l\right]+\frac{\partial}{\partial x}\left[\alpha\rho_g u_g^2+(1-\alpha)\rho_l u_l^2+p\right]=s_m, \tag{2.12b}$$

$$\frac{\partial}{\partial t}\left[\alpha E_g+(1-\alpha)E_l\right]+\frac{\partial}{\partial x}\left[\alpha E_g u_g+(1-\alpha)E_l u_l+u_m p\right]=s_e. \tag{2.12c}$$

The total mass of the mixture is conserved, although there is mass transfer between the phases, a source term is not required to model the change phase, unlike what occurs in the system (2.9a)-(2.9d). The system of Eqs. (2.12a)-(2.12c) is in mechanical and thermal equilibrium, but a dynamic disequilibrium is introduced into the mixture. When $u_g=u_l$ is adopted, it reduces to the homogeneous equilibrium model (HEM), which is in full thermodynamic equilibrium.

2.2.1 Closure laws

There are more dependent variables than equations in the system (2.12a)-(2.12c). Five constitutive equations are required. One of them is the kinematic relation between the phases, presented in Eq. (2.8). The other closure laws are obtained from the equation of state used to calculate thermodynamic properties.

For each phase $k=l$, g, thermodynamic properties are calculated using the Noble-Abel Stiffened Gas (NASG) equation of state [37]. Expressions for pressure p, density ρ_k, specific internal energy e_k and speed of sound c_k for each phase are presented below:

$$p(\rho_k,e_k)=\rho_k(\gamma_k-1)\frac{(e_k-q_k)}{1-\rho_k b_k}-\gamma_k p_{\infty,k}, \tag{2.13a}$$

$$\rho_k(p,T)=\frac{p+p_{\infty,k}}{(\gamma_k-1)C_{v,k}T+(p+p_{\infty,k})b_k}, \tag{2.13b}$$

$$e_k(p,T)=\frac{(p+\gamma_k p_{\infty,k})C_{v,k}T}{p+p_{\infty,k}}+q_k, \tag{2.13c}$$

$$c_k(p,\rho_k)=\sqrt{\frac{\gamma_k(p+p_{\infty,k})}{\rho_k(1-\rho_k b_k)}}, \tag{2.13d}$$

where the parameters γ_k, $p_{\infty,k}$, $C_{v,k}$, q_k and b_k are constant coefficients characteristic of each fluid.

The saturation curve of a pure substance is obtained by equating the Gibbs free energy of the phases, resulting in the following expression linking the saturation pressure and temperature:

$$\ln(p+p_{\infty,g})=A+\frac{(B+Ep)}{T}+C\ln T+D\ln(p+p_{\infty,l}) \tag{2.14}$$

with

$$A = \frac{C_{p,l} - C_{p,g} + q'_g - q'_l}{C_{p,g} - C_{v,g}}, \qquad B = \frac{q_l - q_g}{C_{p,g} - C_{v,g}}, \qquad C = \frac{C_{p,g} - C_{p,l}}{C_{p,g} - C_{v,g}}, \tag{2.15a}$$

$$D = \frac{C_{p,l} - C_{v,l}}{C_{p,g} - C_{v,g}}, \qquad E = \frac{b_l - b_g}{C_{p,g} - C_{v,g}}. \tag{2.15b}$$

Two different fluids were used in the cases presented in this paper: water and refrigerant fluid R410a. Although R410a is a mixture of fluids, its behavior can be modeled as an azeotrope fluid. The coefficients of the NASG equation of state are calculated following the procedure given by Métayer and Saurel [37], using property values from REFPROP [34] as the reference property values. For water in the temperature range $[300-500K]$ and for R410a in the pressure range $[1-2\text{MPa}]$, the NASG coefficients are shown in Table 1 [42].

Table 1: NASG coefficients for water in the temperature range $[300-500K]$ and for R410a in the pressure range $[1-2\text{MPa}]$.

Coefficients	Water		R410a	
	Liquid	Vapor	Liquid	Vapor
$C_{p,k}[J/(kg/K)]$	4286	1317	1614	116
$C_{v,k}[J/(kg/K)]$	3631	857	1612	28
$\gamma_k[-]$	1.18	1.54	1.00	4.12
$p_{\infty,k}[\text{Pa}]$	6646×10^5	0	10390933	0
$b_k[m^3/kg]$	6.85×10^{-4}	0	8.72×10^{-4}	0
$q_k[J/kg]$	-1178108	2175724	-242795	391470
$q'_k[J/(kg.K)]$	0	15620	0	10383

3 Numerical schemes

Both isothermal (2.1a)-(2.1c) and adiabatic (2.12a)-(2.12c) systems of equations of the drift-flux two-phase flow models presented in Section 2 can be written in conservative vector form as follows:

$$\frac{\partial \mathbf{Q}}{\partial t} + \frac{\partial \mathbf{F}}{\partial x} = \mathbf{S}, \tag{3.1}$$

where the vectors of the conserved variables $\mathbf{Q} = \mathbf{Q}^m$, fluxes $\mathbf{F} = \mathbf{F}^m$ and source terms $\mathbf{S} = \mathbf{S}^m$ are, for the isothermal drift-flow model ($m = iso$):

$$\mathbf{Q}^{iso} = \begin{bmatrix} q_0 \\ q_1 \\ q_2 \end{bmatrix} = \begin{bmatrix} \alpha\rho_g \\ (1-\alpha)\rho_l \\ \alpha\rho_g u_g + (1-\alpha)\rho_l u_l \end{bmatrix}, \tag{3.2a}$$

$$\mathbf{F}^{iso} = \begin{bmatrix} f_0 \\ f_1 \\ f_2 \end{bmatrix} = \begin{bmatrix} \alpha\rho_g u_g \\ (1-\alpha)\rho_l u_l \\ \alpha\rho_g u_g^2 + (1-\alpha)\rho_l u_l^2 + p \end{bmatrix}, \tag{3.2b}$$

$$\mathbf{S}^{iso} = \begin{bmatrix} s_0 \\ s_1 \\ s_2 \end{bmatrix} = \begin{bmatrix} 0 \\ 0 \\ s_m \end{bmatrix}, \tag{3.2c}$$

and for the adiabatic drift-flow model with phase change ($m = adi$):

$$\mathbf{Q}^{adi} = \begin{bmatrix} q_0 \\ q_1 \\ q_2 \end{bmatrix} = \begin{bmatrix} \alpha\rho_g + (1-\alpha)\rho_l \\ \alpha\rho_g u_g + (1-\alpha)\rho_l u_l \\ \alpha E_g + (1-\alpha)E_l \end{bmatrix}, \tag{3.3a}$$

$$\mathbf{F}^{adi} = \begin{bmatrix} f_0 \\ f_1 \\ f_2 \end{bmatrix} = \begin{bmatrix} \alpha\rho_g u_g + (1-\alpha)\rho_l u_l \\ \alpha\rho_g u_g^2 + (1-\alpha)\rho_l u_l^2 + p \\ \alpha E_g u_g + (1-\alpha)E_l u_l + u_m p \end{bmatrix}, \tag{3.3b}$$

$$\mathbf{S}^{adi} = \begin{bmatrix} s_0 \\ s_1 \\ s_2 \end{bmatrix} = \begin{bmatrix} 0 \\ s_m \\ s_e \end{bmatrix}. \tag{3.3c}$$

The systems of equations of the drift-flux two-phase models (3.1) can be integrated over a control volume to produce a semi-discrete finite volume formulation. The most challenging part of solving this finite volume formulation is to determine an approximation for the numerical flux $\mathbf{F}_{i+1/2}$ at the cell interface. For an accurate numerical solution, it would be desirable to have an upwind resolution of all the waves inherent in the two-phase model, for example, building an approximate Riemann solver of Roe [43]. However, this is relatively complex, even for simpler drift-flux two-phase models [22,45]. For the drift-flux two-phase models considered in this paper, since $u_g \neq u_l$, there is no tractable exact expression for the Jacobian matrix, as well as for the eigenvalues of the system of equations [50]. Consequently, the use of numerical schemes that only make explicit use of the eigenvalues associated with nonlinear waves also becomes computationally complicated.

The high-order compact finite difference scheme, described in the next section, becomes an attractive alternative on these occasions, as it does not make use of any wave propagation information from the system of equations.

3.1 High-order compact finite difference schemes

Compact schemes provide a finite difference approximation for the first derivative of the fluxes (3.1) based on linear combinations of values centered on neighboring cells. These schemes use a compact stencil and are characterized by a high spectral resolution [33]. For any scalar quantity f, the finite difference approximation of the first spatial derivative at node i is obtained by following formula [33]:

$$\alpha \left.\frac{\partial f}{\partial x}\right|_{i-1} + \left.\frac{\partial f}{\partial x}\right|_i + \alpha \left.\frac{\partial f}{\partial x}\right|_{i+1} = a\frac{f_{i+1} - f_{i-1}}{2\Delta x} + b\frac{f_{i+2} - f_{i-2}}{4\Delta x} + c\frac{f_{i+3} - f_{i-3}}{6\Delta x}, \tag{3.4}$$

where $\alpha = 1/3$, $a = 14/9$, $b = 1/9$ and $c = 0$ for the sixth-order scheme. At points close to the domain boundaries, fifth-order one-sided formulas are utilized that retain the tridiagonal form of the equation set [24]. For the lower boundary stencil:

$$\frac{\partial f}{\partial x}\bigg|_i + \frac{3}{2}\frac{\partial f}{\partial x}\bigg|_{i+1} = \frac{1}{\Delta x}\left(-\frac{1}{8}f_{i-1} - \frac{11}{6}f_i + \frac{3}{2}f_{i+1} + \frac{1}{2}f_{i+2} - \frac{1}{24}f_{i+3}\right). \tag{3.5}$$

The upper boundary stencil can be obtained by flipping the lower boundary stencil and switching the sign of the stencil coefficients on the right side of expression (3.5).

Compact finite difference schemes are non-dissipative and are thus known to be susceptible to failure due to increasing numerical instability. These difficulties originate from a variety of sources, including mesh non-uniformity, approximate boundary conditions and non-linearity [25]. Thus, to minimize errors from unresolved scales and preserve the stability of the numerical schemes, a high-order compact low-pass spatial filtering scheme [33] is applied to the conserved variables after each time step:

$$\alpha_f \hat{q}_{i-1} + \hat{q}_i + \alpha_f \hat{q}_{i+1} = \sum_{n=0}^{4} \frac{a_n}{2}(q_{i+n} + q_{i-n}), \tag{3.6}$$

where $\hat{q}_i$ is the filtered quantity. An eighth-order filter is obtained with the following coefficients [24]:

$$a_0 = \frac{93 + 70\alpha_f}{128}, \quad a_1 = \frac{7 + 18\alpha_f}{16}, \quad a_2 = \frac{-7 + 14\alpha_f}{32}, \tag{3.7a}$$

$$a_3 = \frac{1 - 2\alpha_f}{16}, \quad a_4 = \frac{-1 + 2\alpha_f}{128}, \tag{3.7b}$$

with the coefficient α_f being a free parameter that satisfies the inequality $-0.5 < \alpha_f \leq 0.5$. In this range, as the parameter α_f is increased, the filtering is more localized to the high wavenumbers. In this paper, the parameter α_f is set to 0.49 unless otherwise noted. High-order one-sided formulas given by Gaitonde and Visbal [24] are used for the near boundary points.

Despite their high spectral resolution, high-order compact schemes cannot be applied directly to flows that contain discontinuities. When high-order filters are applied to flows that contain steep gradients, such as shock waves, contact surfaces and material interfaces, spurious non-physical oscillations are generated that make the simulation unstable. This behavior, associated with the large stencil of the spatial filter, cannot be corrected by a simple adjustment of the filter parameter α_f [55]. Therefore, it is necessary to carry out a special treatment to extend numerical algorithms to problems involving discontinuities.

3.2 Localized Artificial Diffusivity (LAD) method

Cook and Cabot [13, 14] proposed an attractive method for capturing discontinuities that properly removes spurious non-physical oscillations without damping the resolved

scales of the flow. The method is based on the idea of locally adding grid-dependent artificial diffusivity based on a uniformly spaced Cartesian mesh by using high-derivative functions. The capability of this approach to accurately treats shock-turbulence interaction was successfully demonstrated by several authors [20, 30].

The LAD method consists of adding an artificial viscous term τ_{2f} to the momentum and energy equations of the drift-flux two-phase models. This added term takes the form of the viscous stress term of the Navier-Stokes equations:

$$\tau_{2f} = \mu_{2f} \frac{\partial u_m}{\partial x}, \tag{3.8}$$

where μ_{2f} is a grid-dependent artificial viscosity. In order to maintain the high resolution of the numerical scheme, the artificial dissipation introduced has the function of suppressing only the unresolved high frequency scales in a given grid. This is achieved by defining the grid-dependent artificial viscosity μ_{2f} proportional to a r-derivative of the dilatation $(\nabla \cdot u_m)$ as follows [13, 30]:

$$\mu_{2f} = C_{\mu_{2f}} \rho_m f_{sw} \overline{\left| \frac{\partial^r (\nabla \cdot u_m)}{\partial x^r} \right|} (\Delta x)^{r+2}, \tag{3.9}$$

where $C_{\mu_{2f}}$ is a dimensionless user-specified constant and r is a integer number. The term f_{sw} is a switching function (shock sensor) that is designed to remove unnecessary artificial viscosity in the region without shocks and localize it near shock waves. This term is defined following Kawai et al. [30] as $f_{sw} = H(-\nabla \cdot u_m)$, where H is the Heaviside function. To eliminate cusps introduced by the absolute value operator, a Gaussian filter denoted by the overbar $\overline{f}$ is applied to the expression (3.9). The filter defined by Cook and Cabot [13] has the form:

$$\overline{f}_i = \frac{3565}{10368} f_i + \frac{3091}{12960} (f_{i+1} + f_{i-1}) + \frac{1997}{25920} (f_{i+2} + f_{i-2})$$
$$+ \frac{149}{12960} (f_{i+3} + f_{i-3}) + \frac{107}{103680} (f_{i+4} + f_{i-4}). \tag{3.10}$$

At the near boundary points, for a non-periodic boundary condition, the value f_i is mirrored across the domain boundaries [29].

The r-order of the dilatation derivative must be sufficiently high so that the artificial viscosity term μ_{2f} is important in the location near the shock waves and close to zero in the rest of the flow. In the present study, the order of the derivative is set to $r = 4$ [7, 14, 29, 31]. The fourth derivative is evaluated using a fourth-order compact finite difference formula [33]:

$$\frac{1}{4} \frac{\partial^4 f}{\partial x^4} \bigg|_{i-1} + \frac{\partial^4 f}{\partial x^4} \bigg|_i + \frac{1}{4} \frac{\partial^4 f}{\partial x^4} \bigg|_{i+1} = \frac{3}{2} \left(\frac{f_{i+2} - 4f_{i+1} + 6f_i - 4f_{i-1} + f_{i-2}}{\Delta x^4} \right). \tag{3.11}$$

At near boundary points, high-order one-sided explicit formulas given by Kawai and Lele [29] are utilized. In the current study, the dimensionless user-specified constant is set to $C_{\mu_{2f}} = 1.5$ unless otherwise stated.

Since in the LAD method the artificial viscosity term is based only on the mixture velocity derivative, contact discontinuities (density) are not detected by expression (3.9). Often artificial mass diffusivity χ are added to the mass equations in order to capture such contact discontinuities numerically. These terms are modeled following the work of [20, 51] and are extended here for application in two-phase flows [2].

The artificial terms added to the gas (2.1a) and liquid (2.1b) mass equations of the isothermal drift-flux model are:

$$\mathcal{A}_g = \chi_g \frac{\partial \alpha \rho_g}{\partial x}, \qquad\qquad \chi_g = C_{\rho_g} \overline{\frac{c_m}{\rho_g} \left| \frac{\partial^r \alpha \rho_g}{\partial x^r} \right|} (\Delta x)^{r+1}, \qquad (3.12a)$$

$$\mathcal{A}_l = \chi_l \frac{\partial (1-\alpha) \rho_l}{\partial x}, \qquad\qquad \chi_l = C_{\rho_l} \overline{\frac{c_m}{\rho_l} \left| \frac{\partial^r (1-\alpha) \rho_l}{\partial x^r} \right|} (\Delta x)^{r+1}, \qquad (3.12b)$$

where the expression of the speed of sound of the mixture c_m is given in [45]. Numerical experiments led to the choice $C_{\rho_g} = C_{\rho_l} = 0.1$. The suggested values for the constants of the LAD model are function of the spatial discretization and filtering scheme. These values were adopted in this paper because they provided robust results in capturing discontinuities, but may change for other implementations of the LAD method.

With the application of the LAD method in the isothermal drift-flux model (2.1a)-(2.1c), the flux vector is written as:

$$\mathbf{F} = \begin{bmatrix} f_0 \\ f_1 \\ f_2 \end{bmatrix} = \begin{bmatrix} \alpha \rho_g u_g - \mathcal{A}_g \\ (1-\alpha) \rho_l u_l - \mathcal{A}_l \\ \alpha \rho_g u_g^2 + (1-\alpha) \rho_l u_l^2 + p - \tau_{2f} \end{bmatrix}. \qquad (3.13)$$

Additionally, an artificial term for capturing contact discontinuities is also added to the mixture mass equation of the drift-flux model with phase change:

$$\mathcal{A}_m = \chi_m \frac{\partial \rho_m}{\partial x} \quad \text{and} \quad \chi_m = C_{\chi_m} \overline{\frac{c_m}{\rho_m} \left| \frac{\partial^r \rho_m}{\partial x^r} \right|} (\Delta x)^{r+1}, \qquad (3.14)$$

where c_m is the speed of sound of the mixture given by Eq. (3.21). Previous numerical experiments showed that choosing $C_{\chi_m} = 0.05$ was sufficient to capture contact discontinuities. With the application of the LAD method in the system of equations of the adiabatic drift-flux model with phase change (2.12a)-(2.12c), the flux vector becomes:

$$\mathbf{F} = \begin{bmatrix} f_0 \\ f_1 \\ f_2 \end{bmatrix} = \begin{bmatrix} \alpha \rho_g u_g + (1-\alpha) \rho_l u_l - \mathcal{A}_m \\ \alpha \rho_g u_g^2 + (1-\alpha) \rho_l u_l^2 + p - \tau_{2f} \\ \alpha E_g u_g + (1-\alpha) E_l u_l + (p - \tau_{2f}) u_m \end{bmatrix}. \qquad (3.15)$$

The artificial diffusivity terms are inserted only in the calculation of the flux vector. The system of equations of the drift-flux two-phase models to be solved remains the one represented by the form (3.1), but with the flux vector defined by the expressions (3.13) and (3.15), respectively. The LAD method, presented here, is used in conjunction with the methodologies described in Section 3.1. Multidimensional extensions of the method presented in non-Cartesian meshes are available in the literature [29].

3.3 Temporal integration

After spatial discretization, the system of Eqs. (3.1) becomes a set of ordinary differential equations (ODEs) that can be expressed in the form:

$$\frac{d}{dt}\mathbf{Q}_i(t) = -\delta_x \mathbf{F}_i + \mathbf{S}_i = \mathbf{L}(\mathbf{Q}_i), \tag{3.16}$$

where $\delta_x \mathbf{F}_i$ is the finite difference approximation of the spatial derivative of the flux vector. The numerical solution of the set of ODEs (3.16) is advanced in time using a third-order explicit TVD Runge-Kutta method [49]:

$$\mathbf{Q}_i^{n+1/3} = \mathbf{Q}_i^n + \Delta t \mathbf{L}(\mathbf{Q}_i^n), \tag{3.17a}$$

$$\mathbf{Q}_i^{n+2/3} = \frac{3}{4}\mathbf{Q}_i^n + \frac{1}{4}\mathbf{Q}_i^{n+1/3} + \frac{1}{4}\Delta t \mathbf{L}(\mathbf{Q}_i^{n+1/3}), \tag{3.17b}$$

$$\mathbf{Q}_i^{n+1} = \frac{1}{3}\mathbf{Q}_i^n + \frac{2}{3}\mathbf{Q}_i^{n+2/3} + \frac{2}{3}\Delta t \mathbf{L}(\mathbf{Q}_i^{n+2/3}). \tag{3.17c}$$

The maximum stable time step is limited by the CFL condition in the form:

$$\Delta t_{\text{CFL}} = \text{CFL}\frac{\Delta x}{\lambda_{\text{max}}^n}, \tag{3.18}$$

where the eigenvalue λ_{max}^n represents the maximum characteristic velocity of the system of equations at a given time level n. Although in drift-flux two-phase models the possibility of obtaining an analytical expression of the Jacobian matrix is quite difficult, it was possible to obtain approximate expressions for the eigenvalues of the isothermal drift-flux model [45]. Thus, the approximate characteristic velocities of the system of Eqs. (2.1a)-(2.1c) can then be calculated following the formulas presented by Santim and Rosa [45].

As for the adiabatic drift-flux model with phase change, there is neither exact nor approximate expression for the eigenvalues of the system of Eqs. (2.12a)-(2.12c) [50]. The eigenvalue λ_{max}^n usually has the following form:

$$\lambda_{\text{max}} = |u_{\text{max}}| + c_m, \tag{3.19}$$

where u_{max} is the maximum velocity between the phases and c_m is the speed of sound in the gas-liquid mixture. Considering the homogeneous equilibrium model (HEM) in which $u_g = u_l$, Saurel et al. [48] obtained an expression for the speed of sound in the gas-liquid mixture given by:

$$\frac{1}{\rho_m c_{HEM}^2} = \frac{\alpha}{\rho_g c_g^2} + \frac{1-\alpha}{\rho_l c_l^2} + T\left[\frac{\alpha\rho_g}{C_{p,g}}\left(\frac{\partial s_g}{\partial p}\right)_{sat}^2 + \frac{(1-\alpha)\rho_l}{C_{p,l}}\left(\frac{\partial s_l}{\partial p}\right)_{sat}^2\right], \tag{3.20}$$

where s_k represents the specific entropy of each phase. The use of expression (3.20) for numerical simulations is not efficient for computational reasons. In addition, this paper

considers that each phase has its own velocity. In the present numerical formulation, the speed of sound of the mixture is used only in the calculation of time step and artificial diffusivity terms. Therefore, it is more convenient for computational purposes to adopt as a reasonable estimate of the speed of sound of the mixture the expression proposed by Wood [47] given in the form:

$$\frac{1}{\rho_m c_m^2} = \frac{\alpha}{\rho_g c_g^2} + \frac{1-\alpha}{\rho_l c_l^2}. \tag{3.21}$$

The expression (3.21) is also valid for homogeneous flow in mechanical equilibrium, but out of thermal and chemical equilibrium. Therefore, the speed of sound (3.21) must always be greater than the speed of sound given by expression (3.20) [21]. This is preferred in numerical calculations, as better stability is guaranteed with this estimate.

When the LAD scheme is used, the maximum stable time step is limited not only by the inviscid CFL condition (3.18), but also by the maximum viscosity and mass diffusivity existing in the domain. Time scales associated with viscosity μ_{2f} (3.9) and mass diffusivity χ_k (Eqs. (3.12a), (3.12b) and (3.14)) are given by [12]

$$\Delta t_{\mu_{2f}} = \min\left(\frac{\rho_m \Delta x^2}{\mu_{2f}}\right) \quad \text{and} \quad \Delta t_{\chi_k} = \min\left(\frac{\Delta x^2}{\chi_k}\right). \tag{3.22}$$

The simulation time step is chosen to be [12]

$$\Delta t = \min\left\{\Delta t_{\text{CFL}}, 0.2\Delta t_{\mu_{2f}}, 0.2\Delta t_{\chi_k}\right\}. \tag{3.23}$$

4 Numerical simulations

In this section, the proposed numerical method is investigated in order to verify its ability to produce accurate and non-oscillating solutions of pressure profiles, fluid velocities and void fraction. Six numerical examples were selected from the literature to validate the implemented methodology to solve isothermal and adiabatic gas-liquid flows with phase change using drift-flux models.

All the computations in this paper have been performed using a CFL number of CFL = 0.6 and a uniform mesh of 200 points, unless otherwise stated. For the numerical solution of the drift-flux models, the sixth-order compact finite difference scheme with the localized artificial diffusivity method is denoted by LAD-C6.

4.1 Isothermal gas-liquid flow

The numerical results presented in this subsection are obtained by solving the system of Eqs. (2.1a)-(2.1c), where it is assumed that there is no mass transfer between the two phases. The first test case is the two-phase shock tube problem, where the slip relation parameters are initially assumed to be constant. The other cases include flow transition

problems with more complex slip relations. The second case refers to the liquid single-phase to gas-liquid two-phase transition. The third test case, in addition to initially considering the liquid single-phase to gas-liquid two-phase transition, also considers a return transition from gas-liquid two-phase to liquid single-phase flow.

Comparisons with the centred FORCE scheme [52] and the finite volume AUSM scheme [35], both using second-order MUSCL reconstruction [54] will also be provided. The comparison with the FORCE scheme is interesting because, like the LAD-C6 scheme, the FORCE scheme does not make explicit use of wave propagation information in the construction of the numerical flux. The AUSM scheme only makes explicit use of the eigenvalues associated with nonlinear waves, so it is possible to apply it to solve the isothermal drift-flux model using the approximate eigenvalues obtained by Santim and Rosa [45]. Results with the MUSCL-FORCE and MUSCL-AUSM schemes are obtained using the van Leer [53] limiter.

4.1.1 Two-phase shock tube

The gas-liquid shock tube problem considered consists of a shock-contact-shock solution. This case was previously studied in references [17, 22], assuming that the density of the liquid is constant $\rho_l = 1000\text{kg/m}^3$ and neglecting the wall-friction force F_w, so that no source terms are used in the model. In addition, the slip relation (2.8) is used with parameters $C_0 = 1.07$ and $v_d = 0.2162$. The speed of sound in the gas phase is $c_g = \sqrt{10^5}\text{m/s}$. A horizontal tube of length 100m initially is separated in a left and right state at $x_0 = 50\text{m}$. The initial conditions are:

$$\alpha_L = 0.55, \qquad \alpha_R = 0.55, \qquad p_L = 80450.0\text{Pa}, \qquad p_R = 24282.0\text{Pa}, \quad (4.1a)$$

$$u_{g_L} = 12.659\text{m/s}, \quad u_{g_R} = 1.181\text{m/s}, \quad u_{l_L} = 10.370\text{m/s}, \quad u_{l_R} = 0.561\text{m/s}. \quad (4.1b)$$

The numerical solution of the problem is obtained at time $t = 1.0\text{s}$ and the reference solution was given by Flåtten and Munkejord [22] with a proposed second-order Roe scheme. Fig. 1 shows a comparison of the numerical results obtained with the reference solution. Overall, numerical schemes successfully capture all discontinuities and show good agreement with the reference solution. In particular, this fact demonstrates the validity of using the expressions of approximate eigenvalues from the system of equations [45] in the MUSCL-AUSM scheme. The MUSCL-FORCE and MUSCL-AUSM schemes presents non-oscillatory solutions for all variables. However, the MUSCL-FORCE scheme becomes more dissipative at contact discontinuities. The LAD-C6 scheme successfully captures the contact discontinuity and shock wave without generating significant spurious oscillations.

4.1.2 Transition from liquid single-phase to gas-liquid two-phase flow

This numerical experiment, proposed by Evje and Fjelde [18], aims to verify whether the numerical model can predict the displacement of a gas pocket in a liquid medium. For
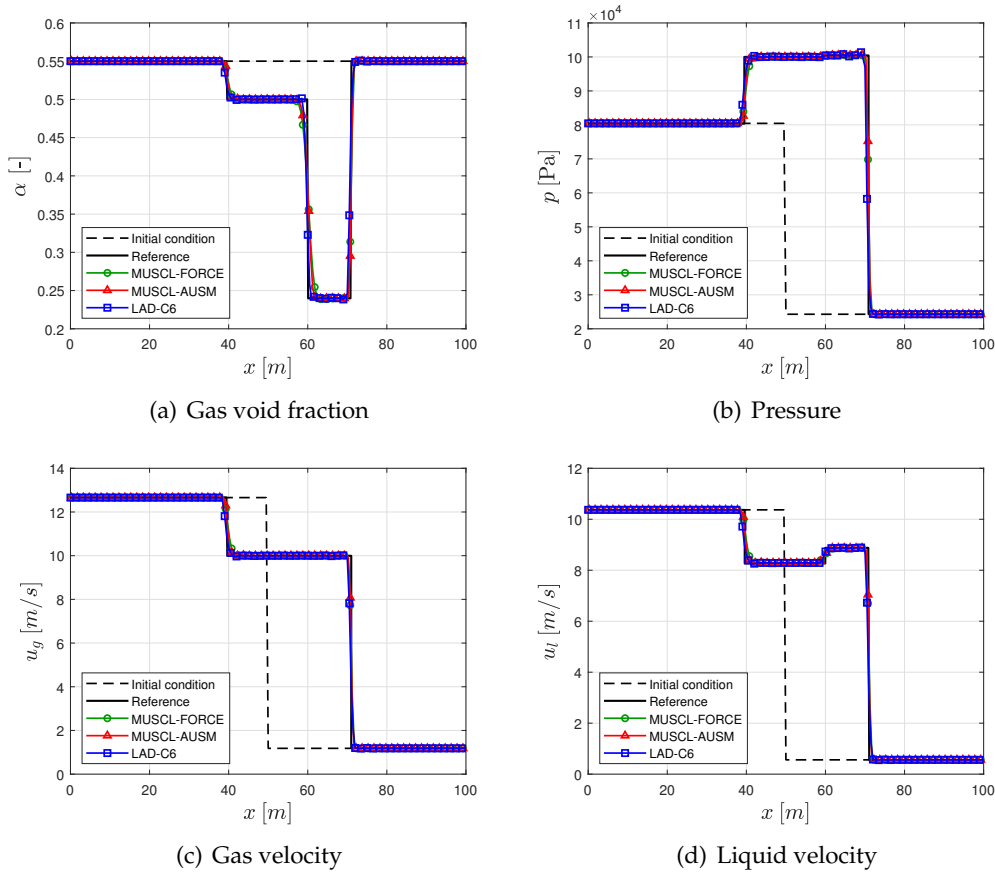
(a) Gas void fraction

(b) Pressure

(c) Gas velocity

(d) Liquid velocity

Figure 1: Numerical solution of the gas-liquid shock tube problem at time $t = 1.0$s.

this, Evje and Fjelde [18] considered a more complex slip relation as a function of the void fraction, similar to that used to model flows in the slug pattern. In this case:

$$C_0 = 1.0, \quad v_d = v_d(\alpha) = 0.5\sqrt{1-\alpha}. \qquad (4.2)$$

The problem consists of a horizontal duct of length 1000m and internal diameter 0.1m. Initially, the duct is filled with stagnant liquid, almost pure with $\alpha = 1 \times 10^{-5}$. Following Evje and Fjelde [18], the physical properties of the gas and liquid used in the flow transition problems are given in Table 2 and a simple friction source term was assumed as $F_w = 32u_m\mu_m/D^2$.

The simulation details are specified as follows: the gas and liquid mass inflow rates are linearly increased from zero to 0.02kg/s and 3kg/s, respectively during 10s, remaining constant until the end of simulation at 250s. The variations in mass inflow rates over time are summarized in Fig. 2. The outlet pressure is kept constant and equal to 1×10^5Pa. The outflow velocities are obtained by imposing mass conservation of the gas-liquid mix-
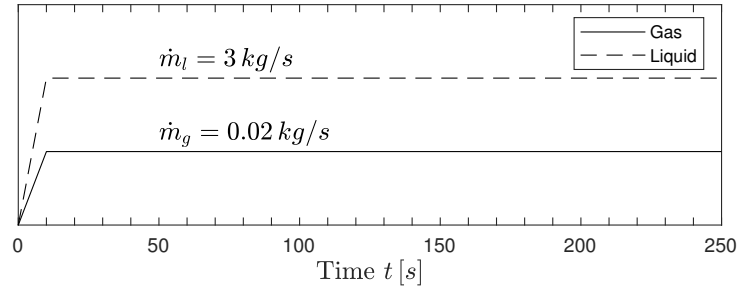
Figure 2: Case 1: Mass inflow rates as a function of time.

Table 2: Physical properties used in flow transition problems.

	Gas	Liquid
Speed of sound $c_k[\text{m/s}]$	316	1000
Reference density $\rho_{k,0}[\text{kg/m}^3]$	–	1000
Reference pressure $p_{k,0}[\text{Pa}]$	–	1×10^5
Viscosity $\mu_k[\text{Pa}\cdot\text{s}]$	5×10^{-6}	5×10^{-2}

ture at the outlet. The reference numerical solution was given by Evje and Fjelde [18], using a second order AUSM scheme with van Leer limiter.

Fig. 3 shows a comparison of the void fraction, pressure, gas velocity and liquid velocity profiles with the results obtained by Evje and Fjelde [18]. It is observed that when injecting the gas phase at the pipeline inlet, a gas pocket tends to form so that for the instant of time $t=250$s, the gas reached approximately the middle of the pipe (see Fig. 3(a)). This fact is reflected in the pressure distribution (Fig. 3(b)), where the difference in slope of the pressure drop is due to the lower head loss of the gases. The results of the MUSCL-AUSM and LAD-C6 schemes are in good agreement with the reference solution, and the discontinuity of void fraction is described well where no oscillations are visible. It is clear that the MUSCL-FORCE scheme is rather diffusive and strongly smears the contact discontinuity. The numerical results indicate that the numerical model is capable of dealing with the transition from liquid single-phase to gas-liquid two-phase flow.

4.1.3 Transition from gas-liquid two-phase to liquid single-phase flow

This flow transition case, also provided by Evje and Fjelde [18], aims to verify the capacity of the numerical model to capture the movement of the gas flow, created between liquid pockets, along the pipeline. In order to evaluate the stability and convergence properties for complex slip relations in the transition from gas-liquid two-phase to liquid single-phase flow, the same relation (4.2) is used for the slip between phases.

The flow configurations are the same as defined in the previous case, changing only the variation of the mass flow rates at the entrance of the pipeline. Fig. 4 summarizes the variations in mass inflow rates over time. The gas and liquid mass flow rates increase
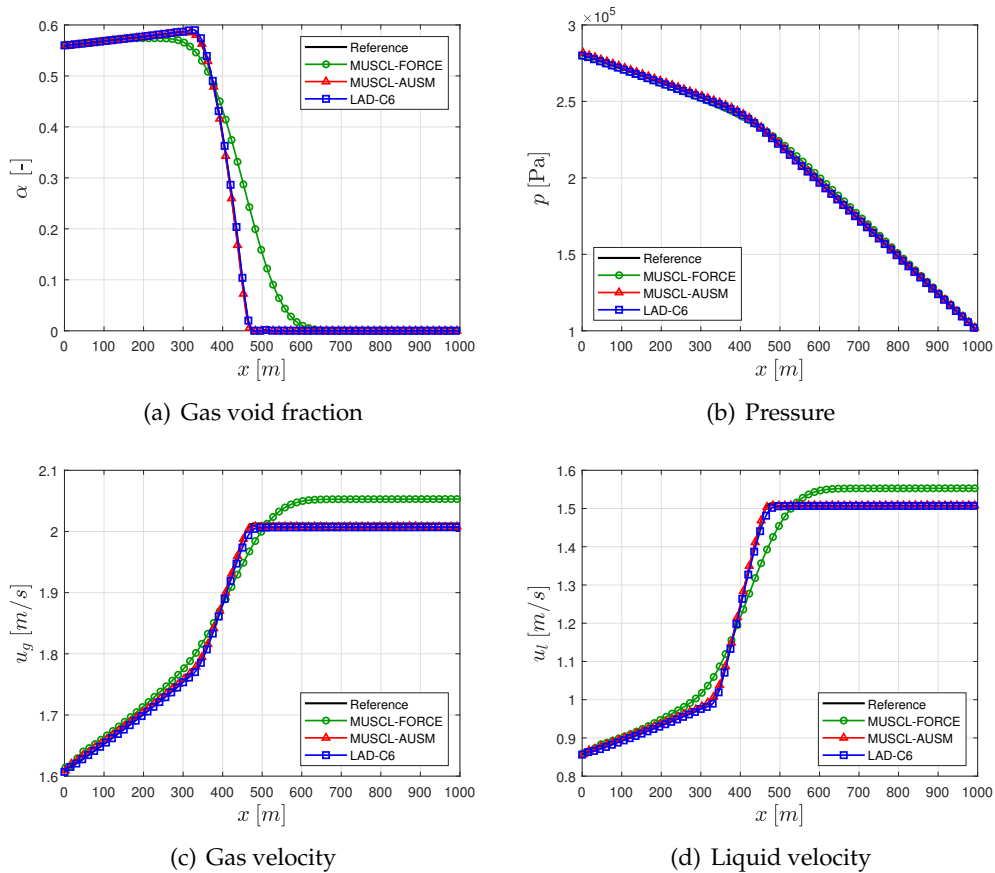
(a) Gas void fraction

(b) Pressure

(c) Gas velocity

(d) Liquid velocity

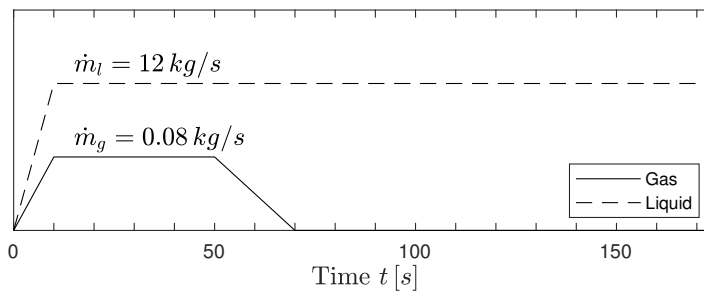Figure 3: Numerical results of liquid single-phase to gas-liquid two-phase transition problem at $t = 250$s.

Figure 4: Case 2: Mass inflow rates as a function of time.

from zero to 0.08kg/s and 12kg/s respectively in 10s. After 50s the gas mass flow rate decreases to zero in 20s, while the liquid mass flow rate remains constant throughout the whole simulation. The simulation ends at 175s.
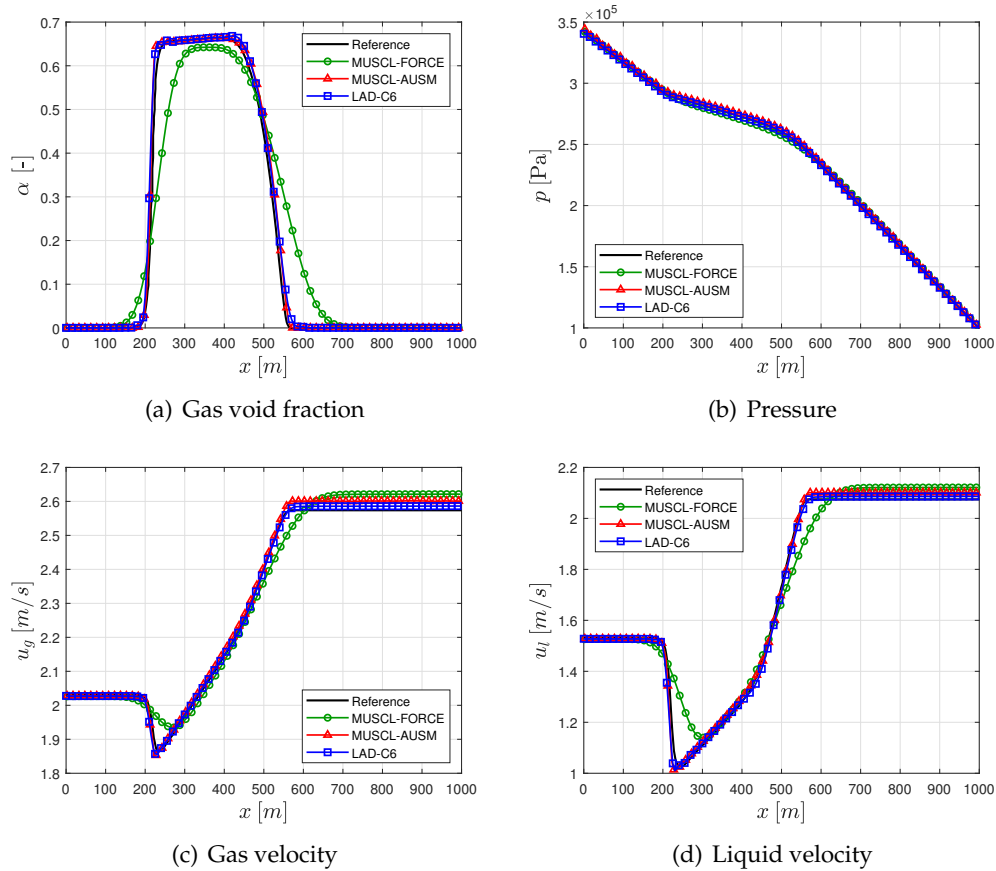
(a) Gas void fraction

(b) Pressure

(c) Gas velocity

(d) Liquid velocity

Figure 5: Numerical results of gas-liquid two-phase to liquid single-phase transition problem at $t=175$s.

Fig. 5 presents the results obtained with the MUSCL-FORCE, MUSCL-AUSM and LAD-C6 schemes in comparison with the reference solution given by Evje and Fjelde [18] at time $t=175$s. It is observed, from the void fraction profile (Fig. 5(a)), that the numerical model is able to deal with the return to the liquid single-phase flow after a period of gas-liquid two-phase flow. As in the previous case, an excellent agreement can be seen between the results for the pressure distribution along the duct (Fig. 5(b)). However, it is obvious that the MUSCL-FORCE scheme is not suitable for this kind of calculation due to its smearing of volume-fraction waves. The result of the LAD-C6 scheme is slightly better compared to the reference solution than the MUSCL-AUSM scheme, especially for the gas and liquid velocities in Figs. 5(c) and 5(d) respectively. In particular, it is observed that the LAD-C6 scheme does not introduce any oscillations at the transition zones between gas-liquid two-phase flow and liquid single-phase flow.

4.2   Adiabatic gas-liquid flow with phase change

This subsection deals with the gas-liquid flows with phenomena of condensation or vaporization of a pure substance. The numerical results are obtained by solving the system of Eqs. (2.12a)-(2.12c). To validate the transient numerical method, shock tube problems containing liquid water and its own vapor, where phase change occurs, are considered. Finally, an upward vertical gas-liquid flow of R410a in steady-state is also considered. The numerical solutions of the MUSCL-FORCE and LAD-C6 schemes are compared only in the shock tube problems.

4.2.1   Shock tube with a mixture containing mainly liquid water

The shock tube problem considered was proposed by Chiapolino et al. [10]. The authors used the homogeneous relaxation model (HRM) and developed a relaxation algorithm for the phase transition. The tube is 1m long and have an initial discontinuity located at 0.5m. Following Chiapolino et al. [10], the homogeneous model was chosen for these simulations, implying the choice of drift-flux parameters $C_0 = 1.0$ and $v_d = 0.0$ in the slip relation (2.8). The thermodynamic properties of liquid water were evaluated using the NASG equation of state. No source terms were considered in these simulations.

The initial conditions of the problem correspond to both saturated liquid and vapor each time a two-phase mixture is present initially. Given the initial pressures and mass fractions, the initial temperatures are calculated with Eq. (2.14), and thermodynamic properties are obtained from the equations of state. The velocity in the initial condition is given by $u_l = u_g = u_m = 0$m/s and a gas-liquid mixture with an initial liquid mass fraction of $Y_l = 0.8$ is considered throughout the tube. The initial pressure condition is $p_L = 2 \times 10^5$Pa for $x \leq 0.5$m and $p_R = 1 \times 10^5$Pa for $x > 0.5$m. Due to the hypothesis of pure substance in the saturation condition, the discontinuity of pressure in the initial condition leads to discontinuities in the other thermodynamic properties. The results obtained by Chiapolino et al. [10] using the first-order HLLC Riemann solver are used for comparison.

Fig. 6 shows a comparison of the results of the MUSCL-FORCE and LAD-C6 schemes with the solution presented by Chiapolino et al. [10]. A condensation process can be observed in the shock wave, while an evaporation process (cavitation) occurs through the expansion wave. The agreement between the results is quite satisfactory, despite the first-order results of the reference solution. In particular, the LAD-C6 scheme successfully captures the present discontinuities without generating considerable oscillations.

4.2.2   Shock tube with transition to pure gas

This second shock tube problem, also formulated by Chiapolino et al. [10], is similar to the previous one, but involves the disappearance of the liquid phase. The initial conditions are similar: velocity is given by $u_l = u_g = u_m = 0$m/s along the tube and a discontinuity in pressure is considered with $p_L = 2 \times 10^5$Pa for $x \leq 0.5$m and $p_R = 1 \times 10^5$Pa for $x > 0.5m$. However in this problem, an initial liquid mass fraction of $Y_l = 0.01$ is considered

(a) Mixtury density
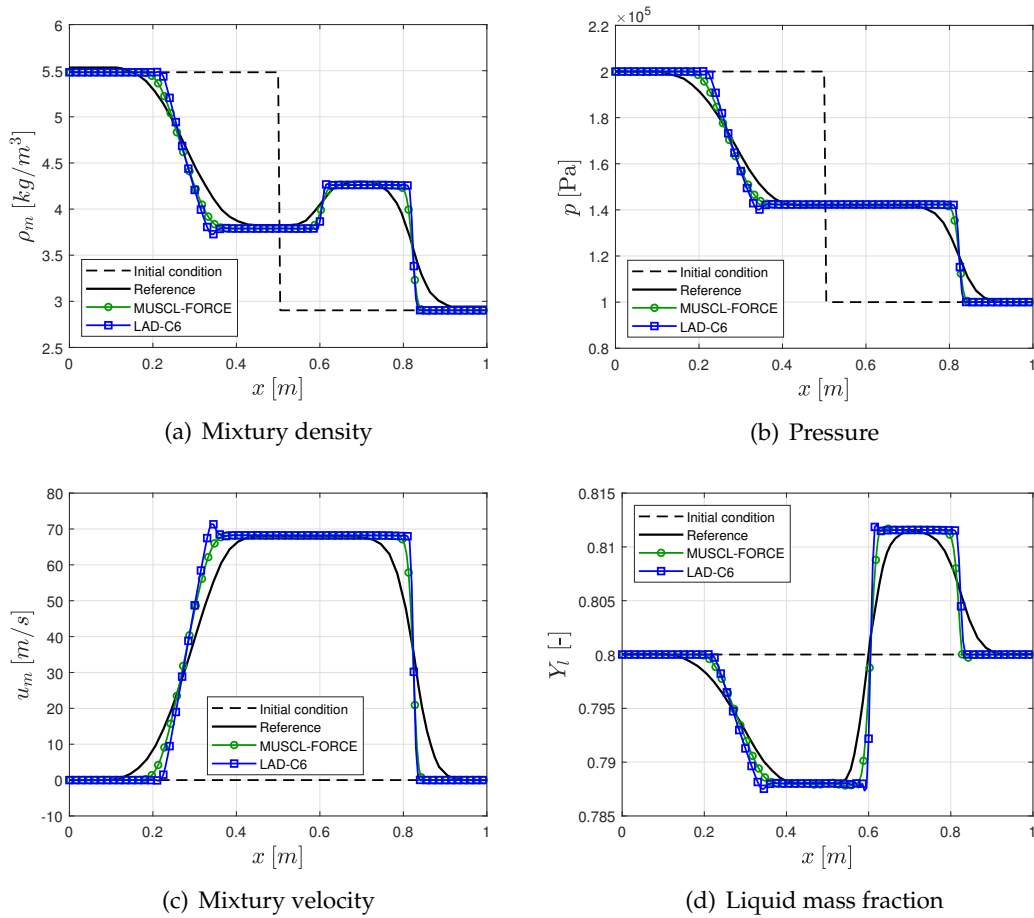
(b) Pressure

(c) Mixtury velocity

(d) Liquid mass fraction

Figure 6: Numerical solution of the shock tube problem with a two-phase mixture composed mainly of liquid water at $t = 1.5$ms.

throughout the tube, which leads to the condition of pure gas in certain regions of the domain.

Numerical results are shown in Fig. 7. Again, good agreement with the reference solution is obtained. Here, the shock compression of the gas-liquid mixture produces total evaporation of the liquid phase. On the other hand, the expansion wave produces a condensation process. It is noteworthy that small differences between the numerical solutions may exist due to the different ways of evaluating the thermodynamic properties and the order of accuracy of the numerical schemes used. As seen in the previous subsection, the MUSCL-FORCE scheme also smeared the rarefaction wave, but perhaps less dramatically than for contact discontinuities. The transition to pure gas is captured with the LAD-C6 scheme without generating spurious oscillations.
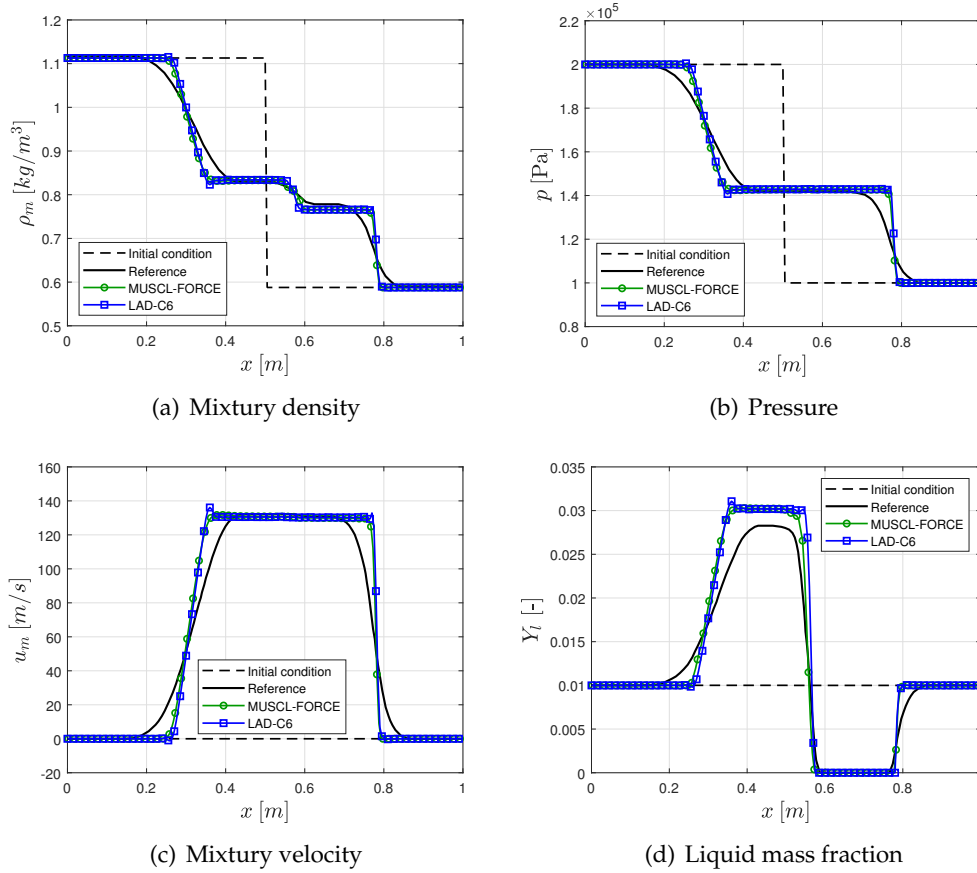
(a) Mixtury density

(b) Pressure

(c) Mixtury velocity

(d) Liquid mass fraction

Figure 7: Numerical solution of the shock tube problem with a two-phase mixture involving a transition to pure gas at $t = 0.5$ms.

4.2.3 Upward vertical gas-liquid flow of R410a

This test case aims to validate the use of source terms and complex nonlinear slip relations in the drift-flux model with phase change. This problem is based on simulations presented by Barbosa [4] with a one-dimensional steady-state model employing a marching procedure. An upward vertical gas-liquid flow of R410a is considered in which a transition between two steady-state conditions is imposed. Thus, in addition to verifying the steady-state solutions of the numerical model, there is also a transient to be analyzed.

The case consists of an upward vertical flow in the slug pattern of a gas-liquid mixture of R410a in a pipe of length $L = 40$m and internal diameter $D = 26$mm. The outlet pressure is kept constant and equal to 1.5MPa. At the inlet, the initial gas and liquid superficial velocities at time $t = 0$s are $j_{g,1} = 0.2$m/s and $j_{l,1} = 0.8$m/s, respectively. These conditions are kept constant until $t_1 = 200$s, being reached the first steady-state condition. Between times $t_1 = 200$s and $t_2 = 250$s, the gas and liquid superficial velocities at the input are varied

Table 3: Constants for the polynomial fit of the surface tension of R410a fluid.

Constant	K_0	K_1	K_2	K_3	K_4	K_5	K_6
Value	22.45	-53.42	115.20	-150.85	108.44	-39.65	5.76

smoothly until reaching the final values of $j_{g,2} = 0.8\text{m/s}$ and $j_{l,2} = 0.2\text{m/s}$, respectively. These values are kept constant until the end of the simulation at $t = 400\text{s}$, reaching a second steady-state condition. The first and second steady-state conditions correspond to two distinct cases simulated by Barbosa [4].

The smooth transition that occurs in $200\text{s} < t < 250\text{s}$ for the phase superficial velocities is performed using a smootherstep function given by [40]:

$$\Phi = 6\psi^5 - 15\psi^4 + 10\psi^3, \tag{4.3}$$

where the local variable Φ and ψ are contained in the interval $[0,1]$ and are related to the physical variables as:

$$\Phi = \frac{j_k - j_{k,1}}{j_{k,2} - j_{k,1}} \quad \text{and} \quad \psi = \frac{t - t_1}{t_2 - t_1}. \tag{4.4}$$

The thermodynamic properties of R410a fluid were evaluated using the NASG equation of state. All source terms were considered in this simulation. The evaluation of the two-phase friction factor requires the viscosities of each phase, which were calculated as proposed by Geller et al. [26]. The slip relation parameters were evaluated according to the correlation of Bhagwat and Ghajar [8]. The surface tension $\sigma[N/m]$ is estimated through a polynomial fit from REFPROP [34]. The fit was made in the interval $[0.03 - 2\text{MPa}]$ in the form:

$$\sigma = \left(\sum_{i=0}^{6} K_i p^i \right) \cdot 10^{-3}, \tag{4.5}$$

where p is the pressure in MPa and K_i are constants given in Table 3 [42].

The history of the mixture specific enthalpy $h_m = (1 - Y_g)h_l + Y_g h_g$, at various positions in the pipeline, is shown in Fig. 8, where Y_g is the gas mass fraction and h_k is the specific enthalpy of each phase. It can be noted that in time interval $[100 - 200\text{s}]$, when the condition at the inlet are $j_{g,1} = 0.2\text{m/s}$ and $j_{l,1} = 0.8\text{m/s}$, the solution is in steady-state and that the mixture specific enthalpy is approximately constant along the pipeline. After 200s, the simulation enters a transient state due to changing inlet conditions. The mixture specific enthalpy starts to vary in both time and space. After 300s, now with inlet conditions of $j_{g,2} = 0.8\text{m/s}$ and $j_{l,2} = 0.2\text{m/s}$, a new steady-state is reached and the mixture specific enthalpy is again approximately constant along the pipeline. Thus, the adiabatic flow hypothesis with constant mixture specific enthalpy in steady-state condition is valid, as adopted by the Barbosa model [4].

Fig. 9 presents the results of the void fraction, pressure and superficial velocities of the phases in the two steady-state conditions. The results of Barbosa [4] are also included
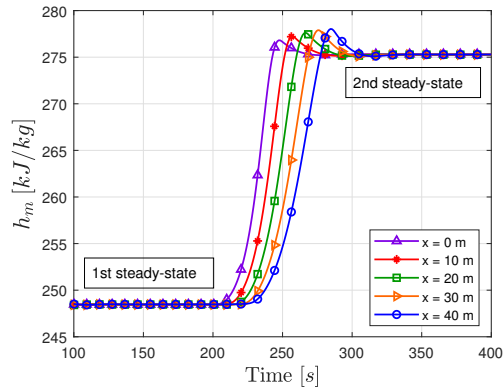
Figure 8: Mixture enthalpy profile for the two steady-state conditions.

(a) Void fraction

(b) Pressure

(c) Gas superficial velocity
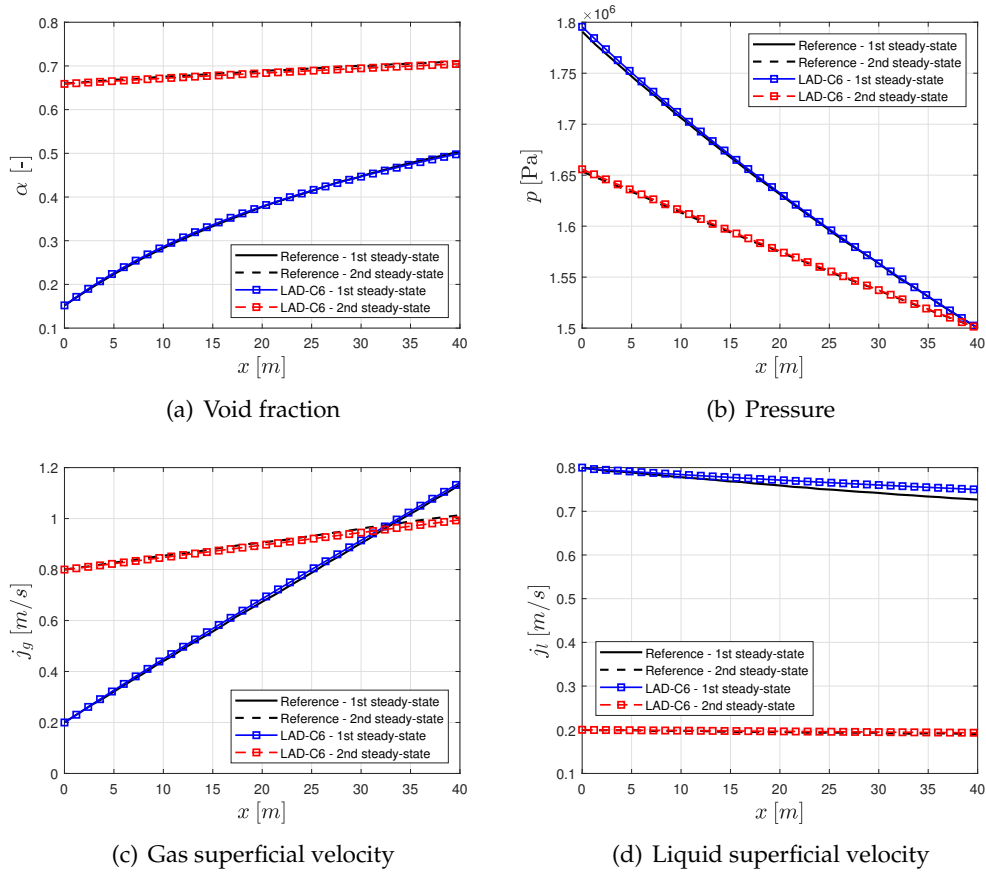
(d) Liquid superficial velocity

Figure 9: Numerical solution of the upward vertical flow of R410a in steady state.

for comparison. As the flow is vertically upward, the pressure drops along the pipeline length (Fig. 9(b)), since the pressure gradient is dominated by the gravitational term. This pressure drop causes part of the liquid phase to evaporate, reducing the liquid mass in the tube and increasing the gas mass. This fact reflects an increase in the void fraction (Fig. 9(a)) and gas superficial velocity (Fig. 9(c)) along the pipeline, while the liquid superficial velocity decreases (Fig. 9(d)). From the comparisons, it can be noticed that the simulation results converge uniformly to the reference solution, showing a good agreement.

5   Conclusions

The purpose of this paper is to validate the numerical methodology used to solve isothermal and adiabatic processes, with evaporation or condensation, in one-dimensional transient gas-liquid flows using drift-flux models. Furthermore, the high-order compact finite difference scheme with the localized artificial diffusivity method (LAD-C6) is extended to capture discontinuities in two-phase flows. The numerical solutions are compared with reference solutions found in the literature.

For the cases of isothermal and adiabatic gas-liquid flows with phase change, the nonlinear hyperbolic systems of the two-phase models cannot be easily solved by classical finite volume methods, such as the Godunov- and Roe-type methods. Even the AUSM scheme, which does not require any calculation of the Jacobian matrix, makes explicit use of eigenvalues associated with the nonlinear waves. The LAD-C6 scheme has become an attractive alternative on these occasions, as it does not make use of the wave propagation information from the system of equations. The proposed LAD-C6 scheme provides accurate approximations of shock waves and contact discontinuities without generating significant spurious oscillations, even for complex slip relations [8, 11]. These essential properties guarantee accurate and simple simulations of realistic transport phenomena. Furthermore, the numerical results obtained demonstrated that the numerical methodology employed is satisfactory for applications in transient gas-liquid flows.

Acknowledgements

References

[1] R. ABGRALL AND R. SAUREL, *Discrete equations for physical and numerical compressible multiphase mixtures*, J. Comput. Phys., 186 (2003), pp. 361–396.

[2] M. ASLANI AND J. D. REGELE, *A localized artificial diffusivity method to simulate compressible multiphase flows using the stiffened gas equation of state*, Int. J. Numer. Methods Fluids, 88 (2018), pp. 413–433.

[3] M. BAER AND J. NUNZIATO, *A two-phase mixture theory for the deflagration-to-detonation transition (ddt) in reactive granular materials*, Int. J. Multiphase Flow, 12 (1986), pp. 861–889.

[4] M. R. BARBOSA, Estudo da Influência da Densidade do gás no Escoamento Bifásico gás-Líquido Usando um Modelo de Mistura, PhD thesis, Faculty of Mechanical Engineering, State University of Campinas, Campinas, Brazil, 2017.

[5] D. BEATTIE AND P. WHALLEY, *A simple two-phase frictional pressure drop calculation method*, Int. J. Multiphase Flow, 8 (1982), pp. 83–87.

[6] K. H. BENDIKSEN, *An experimental investigation of the motion of long bubbles in inclined tubes*, Int. J. Multiphase Flow, 10 (1984), pp. 467–483.

[7] A. BHAGATWALA AND S. K. LELE, *A modified artificial viscosity approach for compressible turbulence simulations*, J. Comput. Phys., 228 (2009), pp. 4965–4969.

[8] S. M. BHAGWAT AND A. J. GHAJAR, *A flow pattern independent drift flux model based void fraction correlation for a wide range of gas-liquid two phase flow*, Int. J. Multiphase Flow, 59 (2014), pp. 186–205.

[9] Z. BILICKI AND J. KESTIN, *Physical aspects of the relaxation model in two-phase flow*, Proceedings of the Royal Society of London. A. Mathematical and Physical Sciences, 428 (1990), pp. 379–397.

[10] A. CHIAPOLINO, P. BOIVIN, AND R. SAUREL, *A simple phase transition relaxation solver for liquid–vapor flows*, Int. J. Numer. Methods Fluids, 83 (2016), pp. 583–605.

[11] J. CHOI, E. PEREYRA, C. SARICA, C. PARK, AND J. KANG, *An efficient drift-flux closure relationship to estimate liquid holdups of gas-liquid two-phase flow in pipes*, Energies, 5 (2012), pp. 5294–5306.

[12] A. W. COOK, *Artificial fluid properties for large-eddy simulation of compressible turbulent mixing*, Phys. Fluids, 19 (2007), p. 055103.

[13] A. W. COOK AND W. H. CABOT, *A high-wavenumber viscosity for high-resolution numerical methods*, J. Comput. Phys., 195 (2004), pp. 594–601.

[14] A. W. COOK AND W. H. CABOT, *Hyperviscosity for shock-turbulence interactions*, J. Comput. Phys., 203 (2005), pp. 379–385.

[15] F. COQUEL, K. E. AMINE, E. GODLEWSKI, B. PERTHAME, AND P. RASCLE, *A numerical method using upwind schemes for the resolution of two-phase flows*, J. Comput. Phys., 136 (1997), pp. 272–288.

[16] P. DOWNAR-ZAPOLSKI, Z. BILICKI, L. BOLLE, AND J. FRANCO, *The non-equilibrium relaxation model for one-dimensional flashing liquid flow*, Int. J. Multiphase Flow, 22 (1996), pp. 473–483.

[17] S. EVJE AND K. K. FJELDE, *Hybrid flux-splitting schemes for a two-phase flow model*, J. Comput. Phys., 175 (2002), pp. 674–701.

[18] S. EVJE AND K. K. FJELDE, *On a rough AUSM scheme for a one-dimensional two-phase model*, Comput. Fluids, 32 (2003), pp. 1497–1530.

[19] I. FAILLE AND E. HEINTZÉ, *A rough finite volume scheme for modeling two-phase flow in a pipeline*, Comput. Fluids, 28 (1999), pp. 213–241.

[20] B. FIORINA AND S. LELE, *An artificial nonlinear diffusivity method for supersonic reacting flows with shocks*, J. Comput. Phys., 222 (2007), pp. 246–264.

[21] T. FLÅTTEN AND H. LUND, *Relaxation two-phase flow models and the subcharacteristic condition*, Math. Models Methods Appl. Sci., 21 (2011), pp. 2379–2407.

[22] T. Flåtten and S. T. Munkejord, *The approximate riemann solver of roe applied to a drift-flux two-phase flow model*, ESAIM: Math. Model. Numer. Anal., 40 (2006), pp. 735–764.

[23] F. França and R. Lahey, *The use of drift-flux techniques for the analysis of horizontal two-phase flows*, Int. J. Multiphase Flow, 18 (1992), pp. 787–801.

[24] D. V. Gaitonde and M. R. Visbal, *High-order schemes for navier-stokes equations: Algorithm and implementation into FDL3DI*, Tech. Rep., US Air Force Research Lab, Aug 1998.

[25] D. V. Gaitonde and M. R. Visbal, *Pade-type higher-order boundary filters for the Navier-Stokes equations*, AIAA J., 38 (2000), pp. 2103–2112.

[26] V. Z. Geller, D. Bivens, and A. Yokozeki, *Viscosity of mixed refrigerants, R404A, R407C, R410A, and R507C*, The International Refrigeration and Air Conditioning Conference, vol. 8, 2000, pp. 399–406.

[27] T. Hibiki and M. Ishii, *One-dimensional drift–flux model for two-phase flow in a large diameter pipe*, Int. J. Heat Mass Transf., 46 (2003), pp. 1773–1790.

[28] G.-S. Jiang and C.-W. Shu, *Efficient implementation of weighted ENO schemes*, J. Comput. Phys., 126 (1996), pp. 202–228.

[29] S. Kawai and S. Lele, *Localized artificial diffusivity scheme for discontinuity capturing on curvilinear meshes*, J. Comput. Phys., 227 (2008), pp. 9498–9526.

[30] S. Kawai, S. K. Shankar, and S. K. Lele, *Assessment of localized artificial diffusivity scheme for large-eddy simulation of compressible turbulent flows*, J. Comput. Phys., 229 (2010), pp. 1739–1762.

[31] S. Kawai and H. Terashima, *A high-resolution scheme for compressible multicomponent flows with shock waves*, Int. J. Numer. Methods Fluids, 66 (2010), pp. 1207–1225.

[32] S. Kuila, T. R. Sekhar, and D. Zeidan, *A robust and accurate riemann solver for a compressible two-phase flow model*, Appl. Math. Comput., 265 (2015), pp. 681–695.

[33] S. K. Lele, *Compact finite difference schemes with spectral-like resolution*, J. Comput. Phys., 103 (1992), pp. 16–42.

[34] E. W. Lemmon, I. Bell, M. L. Huber, and M. O. McLinden, *NIST Standard Reference Database 23: Reference Fluid Thermodynamic and Transport Properties-REFPROP, Version 10.0, National Institute of Standards and Technology*, 2018.

[35] M.-S. Liou and C. J. Steffen, *A new flux splitting scheme*, J. Comput. Phys., 107 (1993), pp. 23–39.

[36] M. D. Lorenzo, P. Lafon, M. D. Matteo, M. Pelanti, J.-M. Seynhaeve, and Y. Bartosiewicz, *Homogeneous two-phase flow models and accurate steam-water table look-up method for fast transient simulations*, Int. J. Multiphase Flow, 95 (2017), pp. 199–219.

[37] O. L. Métayer and R. Saurel, *The Noble-Abel stiffened-gas equation of state*, Phys. Fluids, 28 (2016), p. 046102.

[38] S. T. Munkejord, S. Evje, and T. Flåtten, *The multi-stage centred-scheme approach applied to a drift-flux two-phase flow model*, Int. J. Numer. Methods Fluids, 52 (2006), pp. 679–705.

[39] A. Murrone and H. Guillard, *A five equation reduced model for compressible two phase flow problems*, J. Comput. Phys., 202 (2005), pp. 664–698.

[40] K. Perlin, *Improving noise*, in Proceedings of the 29th annual conference on Computer graphics and interactive techniques–SIGGRAPH 02, ACM Press, 2002.

[41] J. Qiu and C.-W. Shu, *On the construction, comparison, and local characteristic decomposition for high-order central WENO schemes*, J. Comput. Phys., 183 (2002), pp. 187–209.

[42] B. R. Rodrigues, Simulação de Escoamento Gás-Líquido Transiente com Mudança de Fase, PhD thesis, Faculty of Mechanical Engineering, State University of Campinas, Campinas, Brazil, 2020.

[43] P. ROE, *Approximate riemann solvers, parameter vectors, and difference schemes*, J. Comput. Phys., 43 (1981), pp. 357–372.

[44] J. ROMATE, *An approximate riemann solver for a two-phase flow model with numerically given slip relation*, Comput. Fluids, 27 (1998), pp. 455–477.

[45] C. G. S. SANTIM AND E. S. ROSA, *Roe-type riemann solver for gas-liquid flows using drift-flux model with an approximate form of the jacobian matrix*, Int. J. Numer. Methods Fluids, 80 (2015), pp. 536–568.

[46] R. SAUREL AND R. ABGRALL, *A multiphase godunov method for compressible multifluid and multiphase flows*, J. Comput. Phys., 150 (1999), pp. 425–467.

[47] R. SAUREL, P. BOIVIN, AND O. L. MÉTAYER, *A general formulation for cavitating, boiling and evaporating flows*, Comput. Fluids, 128 (2016), pp. 53–64.

[48] R. SAUREL, F. PETITPAS, AND R. ABGRALL, *Modelling phase transition in metastable liquids: application to cavitating and flashing flows*, J. Comput. Phys., 607 (2008), pp. 313–350.

[49] C.-W. SHU, *Total-variation-diminishing time discretizations*, SIAM J. Sci. Stat. Comput., 9 (1988), pp. 1073–1084.

[50] H. B. STEWART AND B. WENDROFF, *Two-phase flow: Models and methods*, J. Comput. Phys., 56 (1984), pp. 363–409.

[51] H. TERASHIMA, S. KAWAI, AND M. KOSHI, *Consistent numerical diffusion terms for simulating compressible multicomponent flows*, Comput. Fluids, 88 (2013), pp. 484–495.

[52] E. F. TORO, Riemann Solvers and Numerical Methods for Fluid Dynamics, Springer-Verlag GmbH, 2009.

[53] B. VAN LEER, *Towards the ultimate conservative difference scheme. II. monotonicity and conservation combined in a second-order scheme*, J. Comput. Phys., 14 (1974), pp. 361–370.

[54] B. VAN LEER, *Towards the ultimate conservative difference scheme. V. a second-order sequel to Godunov's method*, J. Comput. Phys., 32 (1979), pp. 101–136.

[55] M. VISBAL AND D. GAITONDE, *Shock capturing using compact-differencing-based methods*, in 43rd AIAA Aerospace Sciences Meeting and Exhibit, American Institute of Aeronautics and Astronautics, Jan 2005.

[56] N. WEI, C. XU, Y. MENG, G. LI, X. MA, AND A. LIU, *Numerical simulation of gas-liquid two-phase flow in wellbore based on drift flux model*, Appl. Math. Comput., 338 (2018), pp. 175–191.

[57] N. ZUBER AND J. A. FINDLAY, *Average volumetric concentration in two-phase flow systems*, J. Heat Transf., 87 (1965), pp. 453–468.